chemosensors

MDPI

Article

Acoustic Vibration Modes of Gold–Silver Core–Shell Nanoparticles

Tadele Orbula Otomalo [1,2], Lorenzo Di Mario [3], Cyrille Hamon [4], Doru Constantin [4], Francesco Toschi [3], Khanh-Van Do [1], Vincent Juvé [2], Pascal Ruello [2], Patrick O'Keeffe [3], Daniele Catone [3], Alessandra Paladini [3] and Bruno Palpant [1,*]

[1] LuMIn, CNRS, ENS Paris-Saclay, CentraleSupélec, Université Paris-Saclay, 91190 Gif-sur-Yvette, France; tadele_orbula.otomalo@univ-lemans.fr (T.O.O.); khanh-van.do@centralesupelec.fr (K.-V.D.)
[2] Institut des Molécules et Matériaux du Mans, UMR 6283 CNRS, Le Mans Université, 72085 Le Mans, France; vincent.juve@univ-lemans.fr (V.J.); pascal.ruello@univ-lemans.fr (P.R.)
[3] EuroFEL Support Laboratory (EFSL), Istituto di Struttura della Materia-CNR (ISM-CNR), 00100 Rome, Italy; lorenzo.dimario@ism.cnr.it (L.D.M.); francesco.toschi@cnr.it (F.T.); patrick.okeeffe@ism.cnr.it (P.O.); daniele.catone@cnr.it (D.C.); alessandra.paladini@cnr.it (A.P.)
[4] LPS, CNRS, Université Paris-Saclay, 91405 Orsay, France; cyrille.hamon@universite-paris-saclay.fr (C.H.); doru.constantin@universite-paris-saclay.fr (D.C.)
* Correspondence: bruno.palpant@universite-paris-saclay.fr

1. Transmission Electron Microscopy Images of the Samples

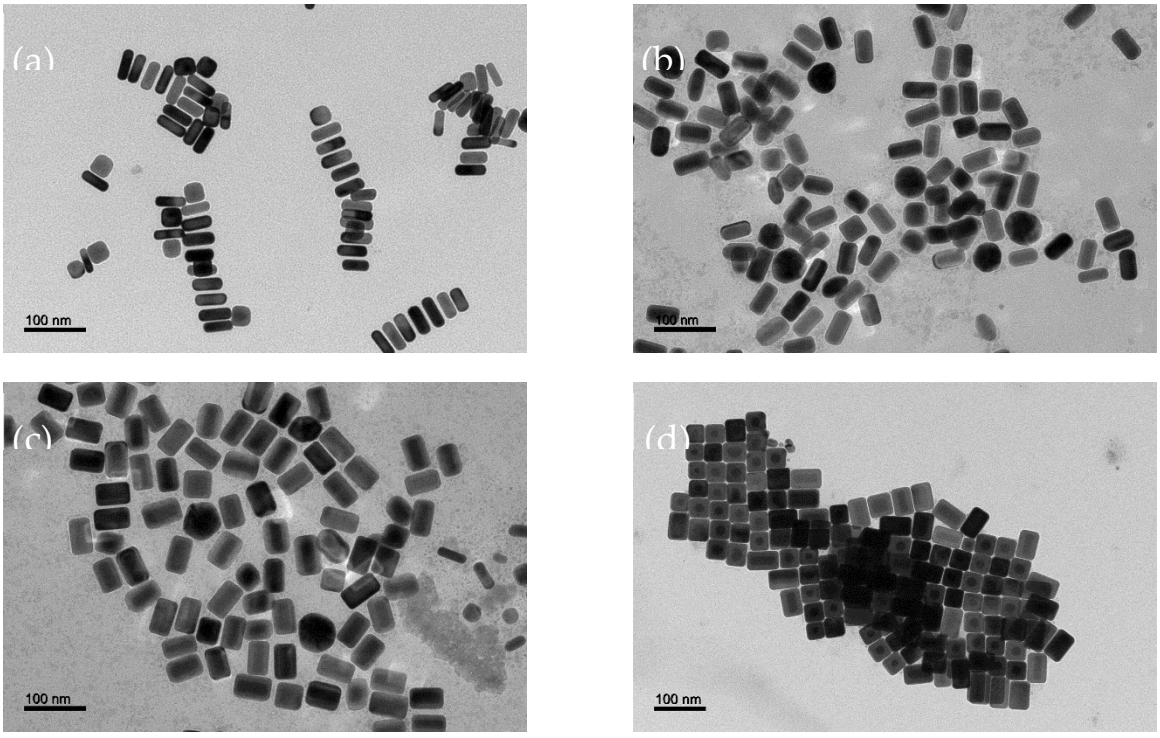

Figure S1. Transmission Electron Microscopy images of 4 samples: bare AuNR (**a**), AuNR@Ag 2eq (**b**), 4eq (**c**), and 8eq (**d**) samples.

2. Stationary Optical Response of the NPs

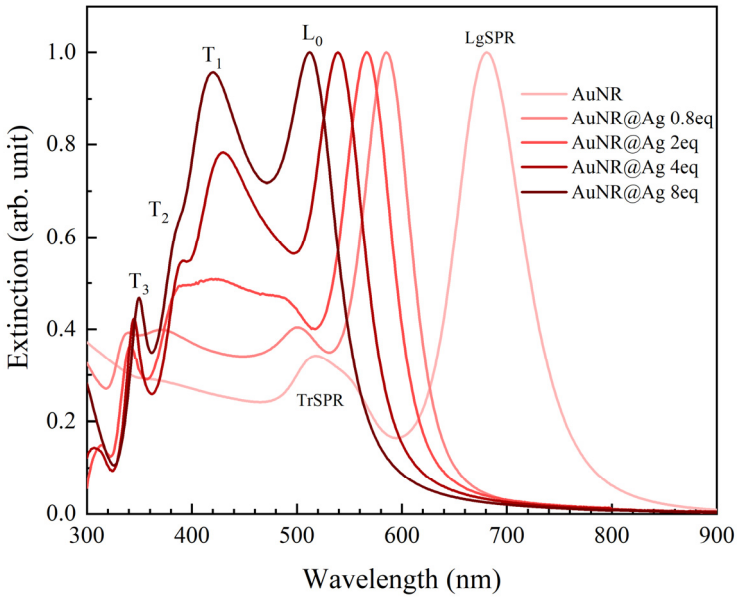

Figure S2. Experimental stationary optical response of the AuNR and AuNR@Ag samples. The plasmon modes that are observed for the bare AuNRs are labelled as longitudinal, LgSPR, and transverse, TrSPR, while those observed for the AuNR@Ag samples are labelled as $\mathbf{L_0}$ and $\mathbf{T_i}$. $\mathbf{L_0}$ is the mode that corresponds to the longitudinal field polarization, while $\mathbf{T_i}$ correspond to the modes of transverse field polarizations, where i = 0 stands for the dipolar mode, and the remaining higher subscripts are for the higher order ones (see Ref. [1] for details). The data is normalized at the LgSPR peak for the AuNR and the $\mathbf{L_0}$ peak for the AuNR@Ag samples.

3. Transient Absorption Spectrum Dynamics

The transient absorption (TA) has been measured over several hundreds of picoseconds. Figures S2a and S2b show the resulting maps for two samples: bare AuNRs and AuNR@Ag 8eq NPs.

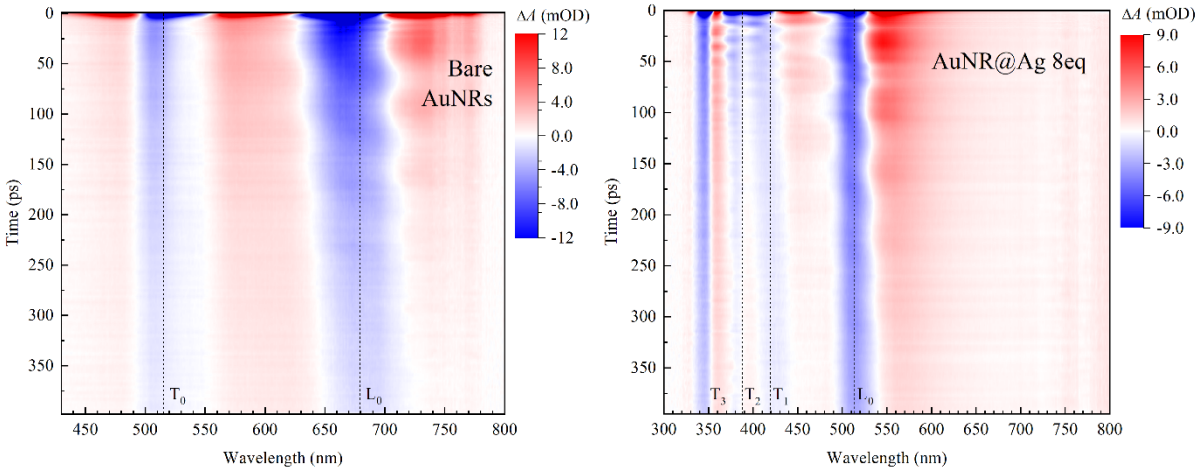

Figure S3. False color map of the time and spectral dependence of the TA (in mOD) of the bare AuNR and AuNR@Ag 8eq samples, respectively, measured by pump-probe spectroscopy over a 400 ps timescale. The color levels and scales have been chosen as to emphasize small signals at long times. The dashed lines denote the spectral location of the resonance modes identified in the stationary spectra.

4. TA Signal Processing before FFT Analysis

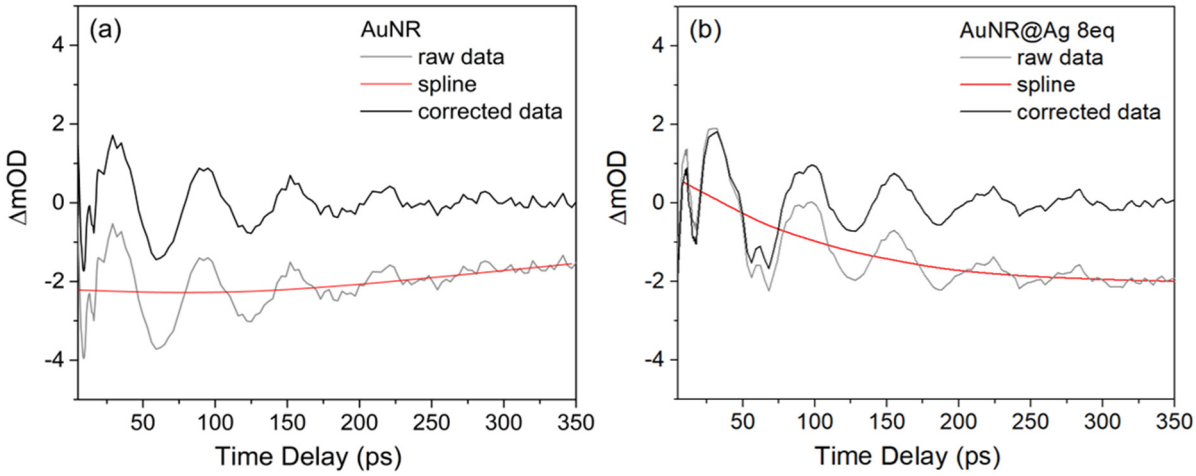

Figure S4. TA signal for the bare AuNR (**a**) and AuNR@Ag 8eq (**b**) samples, monitored at 699 and 526 nm probe wavelengths, respectively. Grey: raw data. Black: data after background removal. The background, stemming from NP cooling down by heat transfer at the interface and heat release in the host medium, is fitted by a spline function (red).

5. Material Properties for the FEM Simulations

Table S1. The material properties of gold and silver that are used in FEM to simulate the acoustic vibrations of the nanoparticles.[2]

	Density, $\boldsymbol{\rho}$	Young's moulus, Y[100]	Poisson's ratio, $\boldsymbol{\nu}$	Coefficient of thermal expansion, $\boldsymbol{\alpha}$
	(kg/m^3)	(Gp)		$(1/K)$
Au	19300	42	0.44	14.2×10^{-6}
Ag	10490	46	0.37	18×10^{-6}

6. Mode Shapes of the Vertex Dominated Oscillation Modes of the AuNR@Ag 2eq NP

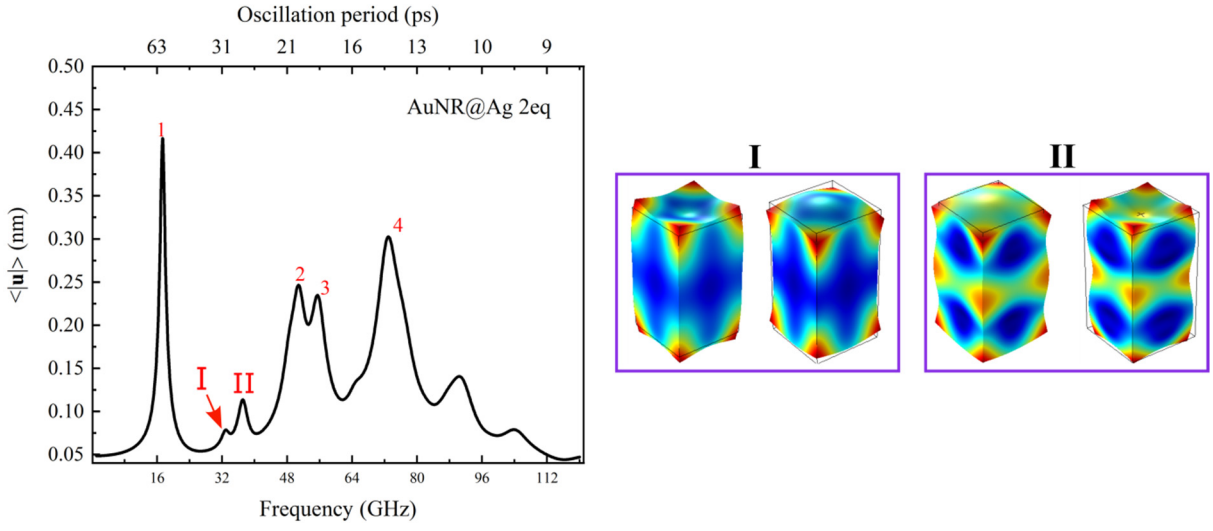

Figure S5. Calculated vibrational mode of the AuNR@Ag 2eq NP as a function of frequency and the mode shapes that correspond to mode-I and mode-II which are dominated by oscillation of the corners.

7. Aspect ratio Dependence of the Vibration Spectrum

In addition to Figure 5 of the main text we plot here the vibration spectra for AuNR@Ag NPs with sharp edges and corners, calculated for different aspect ratios.

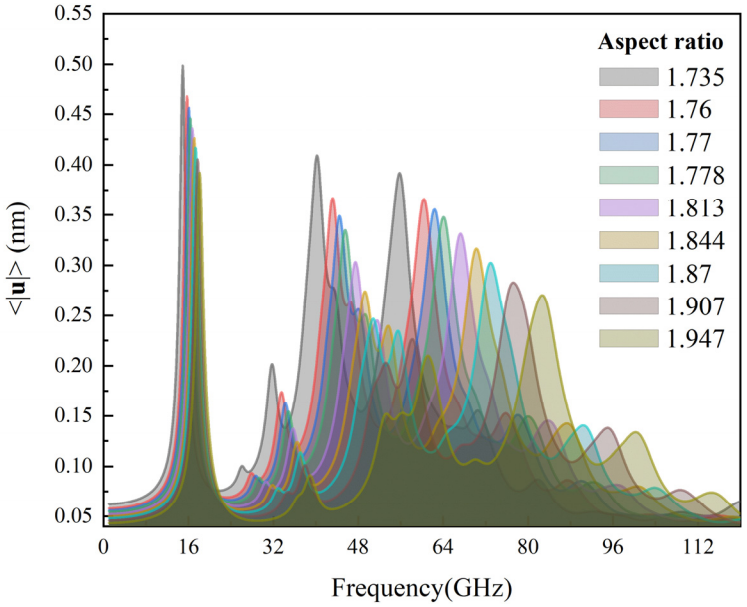

Figure S6. Acoustic vibration spectrum of unrounded (sharp edges and corners) AuNR@Ag NPs for different aspect ratios ranging from 1.735 to 1.947.

8. Rounding Effect

The sharp edges and corners of the AuNR@Ag NPs can be rounded in COMSOL using its fillet operation which performs Boolean operations on multiple spheres (for the corners) and cylinders (for the edges) having the same radius *R*. The vibration modes obtained for the rounded AuNR@Ag 2eq NP for *R* = 2 nm and 5 nm together with the unrounded one are shown here in Figure S6.

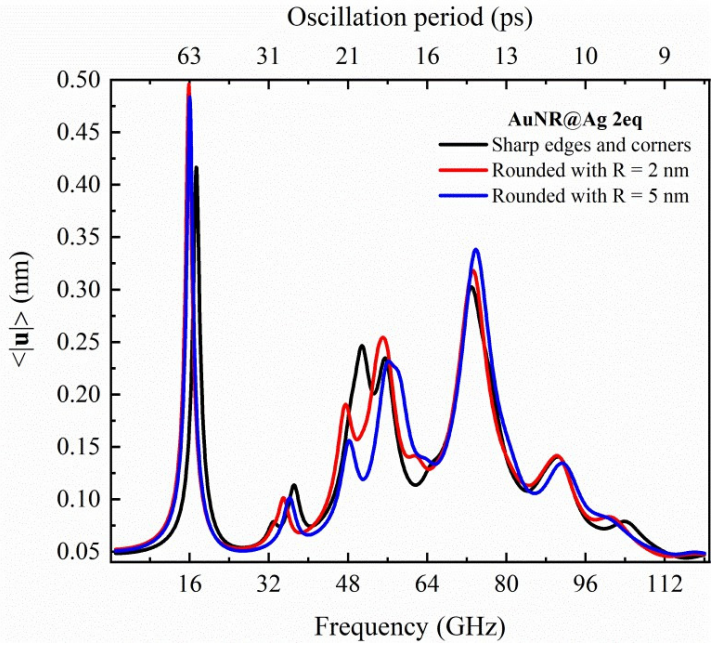

Figure S7. Acoustic vibration spectrum of AuNR@Ag 2eq NP for the unrounded, sharp edges and corners (black curve), and different rounding radii, *R* = 2 nm (red curve) and 5 nm (blue curve).

9. Simulation Design for the Optical Properties of the NPs in ®COMSOL

We took advantage of the geometric symmetry to partition the 3D geometry into four subdomains using two symmetry planes that perpendicularly intersect at its geometrical center. The optical property simulations are then carried out using only a one-fourth of the computational domain (see Figure S7). With this, the expensive memory and storage consequences that would have been encountered if the full 3D geometry was used are reduced. A distributed free tetrahedral meshing is applied in which a very fine mesh is at the NPs. The simulation considers a plane electromagnetic wave with a field polarization along the z-axis and propagating to the positive x-direction (Figure S7). Hence, the symmetry boundary conditions are implemented as follows:

I. Perfect Magnetic Conductor (PMC) along the $y = 0$ symmetry plane ($\mathbf{n} \times \boldsymbol{H}|_{y=0} = 0$), i.e., the tangential component of the magnetic field in the xz-plane is zero.
II. Perfect Electric Conductor (PEC) for $z = 0$ symmetry plane ($\mathbf{n} \times \boldsymbol{E}|_{z=0} = 0$), i.e., the tangential component of the electric field in the xy-plane is zero.

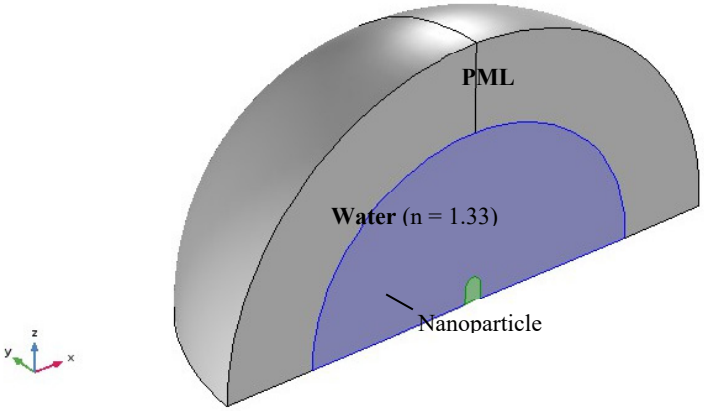

Figure S8. One-fourth of the full 3D geometry which is used for modeling the optical properties in FEM. The PML, the nanoparticle and the host environment (water) are labeled. The internal PML surface (the external surface of the host environment) is taken as the scattering boundary condition *s*.

The model geometry and the symmetry boundary conditions are fixed for all the simulations and only the orientation of the NPs, in front of the incident wave, is adjusted to assess the polarization dependent plasmonic effects. As can be seen from Figure S7, for the longitudinal plasmon, the NP's long axis has to be aligned with the z-direction, and when the transversal plasmonic effect is of interest, it has to be aligned with the y-axis. The optical properties (Eqs. **Error! Reference source not found.** and **Error! Reference source not found.** in the main text) that are obtained in this way are then multiplied by four to account for the contributions of the remaining parts of the 3D geometry.

Figure S8 compares the calculated SPR for AuNR and AuNR@Ag 4eq NPs with their respective experimental data. The model AuNR has a length of 49.0 nm and diameter of 15.8 nm while the AuNR@Ag 4eq NP is given the additional longitudinal Ag thickness of 8 nm and lateral Ag thickness of 19 nm with rounding radius R = 4 nm.

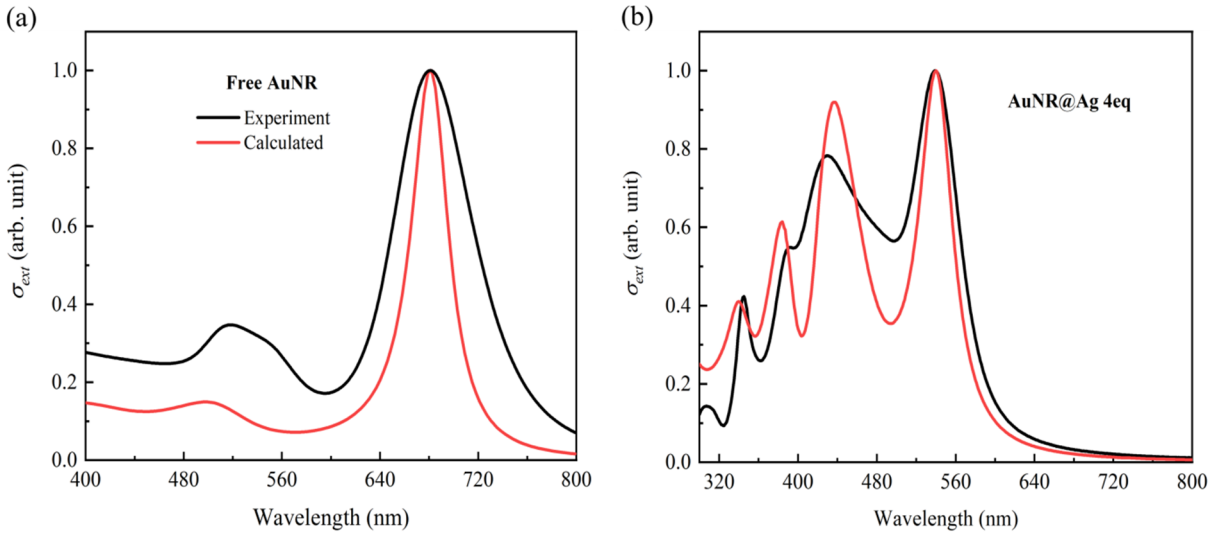

Figure S9. Simulated stationary SPR of the (**a**) AuNR and (**b**) AuNR@Ag 4eq NP using FEM. The red curves are the computed data while the black ones are from the experimental data. All the curves are normalized against their maximum value which is at the lowest photon energy SPR mode.

10. Modification of the Plasma and Interband Transition Frequencies

For small displacement amplitude oscillations, the relative volume change (local expansion) can be evaluated as the trace of the strain tensor,

$$\frac{\Delta V}{V} = e_{xx} + e_{yy} + e_{zz} \quad (1)$$

where the $e_{i,j}$ are the strain tensor elements and the terms with $i \neq j$ are neglected. For this, we extract the oscillation frequency dependent volumetric strain, averaged over the whole NP domain, from the structural mechanics calculation (see § 2.5 and Appendix A in the main text). This functionality of COMSOL also allows us to extract, independently, the volumetric strain values for the AuNR core and Ag shell of the bimetallic NPs, **Error! Reference source not found.**(**b**).

Figure S9 displays the frequency dependent volumetric strain extracted for AuNR and AuNR@Ag 4eq NPfrom COMSOL after the mechanical vibration calculation. The expansion/compression movement of the nanoparticle around the vibrational resonance modes can be observed from the volumetric strain curves. The larger change in volume occurs at the higher-frequency mode for both samples, at the breathing mode for the AuNR and at mode 4 (breathing mode) for the AuNR@Ag 4eq NP.

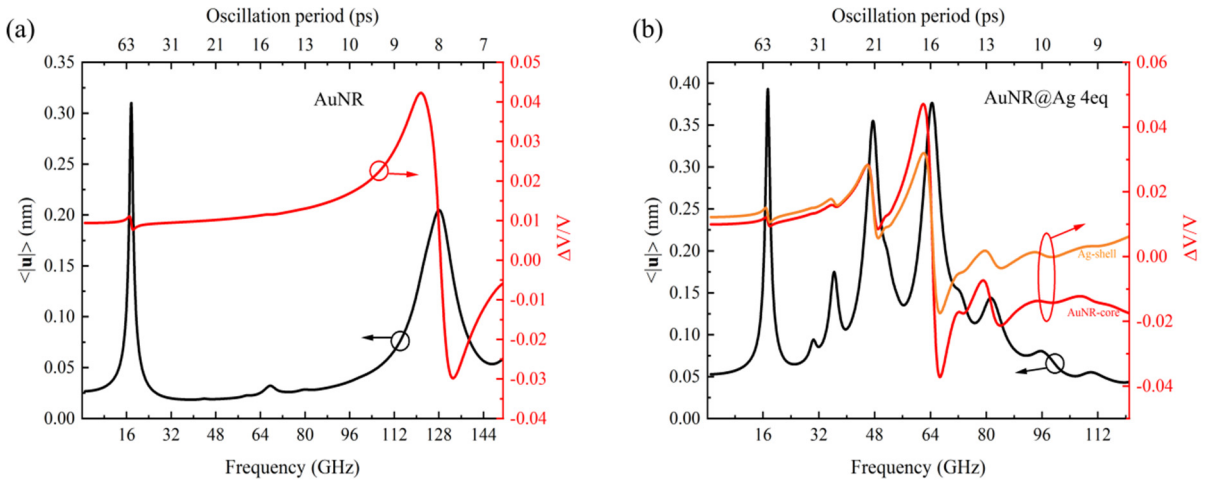

Figure S10. Vibration modes, left *y*-axis (black line) and the vibration induced relative change of volume, right-*y* axis (red, orange lines) of (a) AuNR and (b) AuNR@Ag 4eq NP. In (b), the red curve is for the AuNR-core and the orange curve is for the Ag-shell (both for the right *y*-axis).

The change in the bulk plasma frequency is then estimated from the modification of the free electron density, N', due to the volume change, Eq. **Error! Reference source not found.**:

$$N' = \frac{N}{1 + \frac{\Delta V}{V}}. \quad (2)$$

The contribution of the interband transition frequency variation to the dielectric function of the NPs is modeled using the deformation potential values, ξ_m, at these oscillator frequencies, Eq. **Error! Reference source not found.**. The ξ_m values that we have used for gold and silver are listed in the work of Ahmed et al.[2]

$$\delta E_{0,m} = \xi_m \frac{\delta V}{V}$$
$$\omega'_{0,m} = \omega_{0,m} + \frac{\delta E_{0,m}|e|}{\hbar} \quad (3)$$

where $\delta E_{0,m}$ is change of the interband transition energy associated with m^{th} Lorentzian oscillator. The new Drude–Lorentz model for calculating the modified dielectric function, ε'_r, can then be written as

$$\varepsilon'_r(\omega) = \boldsymbol{\varepsilon_r}(\infty) + \omega'^2_p \sum_{m=0}^{N} \frac{f_m}{\omega'^2_{0,m} - \omega^2 - j\omega\Gamma_m}. \quad (4)$$

Table S2. The parameters used to model the dielectric functions of Au and Ag using the Drude–Lorentz model.[2]

	$\boldsymbol{\varepsilon_r}(\infty)$	$\boldsymbol{\omega_p}$	$\boldsymbol{\omega_{0,1}}$	$\boldsymbol{\omega_{0,2}}$	$\boldsymbol{\Gamma_0}$	$\boldsymbol{\Gamma_1}$	$\boldsymbol{\Gamma_2}$	$\boldsymbol{f_0}$	$\boldsymbol{f_1}$	$\boldsymbol{f_2}$	$\boldsymbol{\xi_1}$	$\boldsymbol{\xi_2}$
				$(10^{15}\ rad/s)$							(eV)	
Au	5.5	13.716	4.428	5.746	0.05979	1.070	1.690	1.039	0.1108	0.3202	−0.8	−9.0
Ag	2.83	13.68	6.538	7.328	0.07969	0.7	0.9	1.029	0.06	0.165	−0.3	−9.0

References

1. Otomalo, T.O.; Di Mario, L.; Hamon, C.; Constantin, D.; Do, K.; O'Keeffe, P.; Catone, D.; Paladini, A.; Palpant, B. Sharp spectral variations of the ultrafast transient light extinction by bimetallic nanoparticles in the near-UV. *Adv. Opt. Mater.* **2021**, *9*, 2001778. https://doi.org/10.1002/adom.202001778.
2. Ahmed, A.; Pelton, M.; Guest, J.R. Understanding how acoustic vibrations modulate the optical response of plasmonic metal nanoparticles. *ACS Nano* **2017**, *11*, 9360–9369. https://doi.org/10.1021/acsnano.7b04789.